Evaluation of E-Field Distribution and Human Exposure for a LTE Femtocell in an Office

Hsing-Yi Chen and Shu-Huan Wen

Department of Communications Engineering
Yuan Ze University, Chung-Li, Taoyuan, 32003, Taiwan
eehychen@saturn.yzu.edu.tw, s1034835@mail.yzu.edu.tw

Abstract ─ Firstly, the finite-difference time-domain (FDTD) method was used to calculate electric fields emitted from a long-term evolution (LTE) femtocell placed at the left-hand side of an empty office at frequencies of 700, 860, 1990, and 2600 MHz. After validating the accuracy of the FDTD method, the FDTD method was used to calculate electric field distributions inside the office, with and without the presence of 20 people and furniture for the LTE femtocell placed near the center of a horizontal plane with a distance of 1.0 m from the ceiling and transmitting a power of 10 dBm. Simulated electric fields at most of the locations on the horizontal plane with a height of 1.0 m above the floor for the office with and without the presence of 20 people and furniture are found in the range of -10 to -30 dBV/m, which means a good signal will be picked up in the office. The maximum power density emitted from the LTE inside the office and maximum localized SAR induced in a standing person are far below the ANSI/IEEE safety standard for public exposure in uncontrolled environments.

Index Terms ─ Electric field, femtocell, LTE, RF exposure, SAR.

I. INTRODUCTION

Recently, indoor wireless networks have increased interest in LTE [1-3] femtocell developments. Through self-optimized configuration and backhaul costs, a LTE femtocell can considerably lower the delivery cost per bit and make it more cost effective for operators to invest in LTE wireless networks. In the near future, LTE femtocells will play a key role in enterprise and metro deployment areas for indoor wireless communications. With the increasing use of indoor wireless networks, there is a challenge to provide a better coverage, higher cell capacity, and higher data rates for mobile applications in the initial design and planning. Therefore, EM field distribution and variability, wave propagation, and path loss of LTE femtocells in different indoor-environments such as offices, airports, railway stations, etc. should be well studied in order to ensure an adequate coverage and good performance for indoor wireless communications. Indoor wave propagation and path loss have been extensively studied, leading to improved coverage and capacity within office buildings [4-11]. The study of indoor EM field distribution and variability for indoor LTE planning and design is not available. EM field strengths at users' locations inside an office should be guaranteed above a threshold level in order to meet the best radio frequency (RF) condition where it is free from interference.

On the other hand, people are great concerned about the potential health hazards due to RF exposure from femtocells in everyday life inside indoor environments such as offices, schools, laboratories, and homes. The biological effect of long-term exposure to RF propagation is simply not known yet with certainty. Additionally, it is impossible to say that exposure to RF radiation, even at levels below safety standards and exposure guidelines, is totally without potential health risks. The potential health hazards resulting from biological effects may include cancers, neurological disorders, allergies, fatigue, sleep disturbance, dizziness, loss of mental attention, headaches, grogginess, memory problems, ringing in the ears (tinnitus), etc. Therefore, the study of long-term exposure due to RF field emission is especially important, since people spend most of their life-time in indoor environments. To access the potential health hazards due to RF fields, the specific absorption rate (SAR) in human bodies in close proximity to LTE femtocells is an important parameter for assessment. Some safety standards and exposure guidelines for human exposure at RF frequencies have been recommended by several national and international organizations such as the National Council on Radiation Protection and Measurements (NCRP) [12], the American National Standards Institute/Institute of Electrical and Electronics Engineers (ANSI/IEEE) [13], and the International Commissions on Non-Ionizing Radiation Protection (ICNIRP) [14]. These safety standards and guidelines define basic restriction and reference levels for human exposure at different frequencies. In the last few years, a few studies have focused on RF exposures in outdoor environments. Some reports about RF

Submitted On: October 12, 2015
Accepted On: February 25, 2016

exposure in outdoor environments are available in the literature [15-19]. A few reports about exposure to RF fields emitted from femtocell in indoor environments are also available in the literature [20-24].

Therefore, it is an important trade-off issue for RF engineers to design a safe indoor environment with LTE femtocells and also to keep RF field intensities above a threshold level for good indoor wireless communications. In this paper, the FDTD method [25] was first used to calculate electric fields emitted from a LTE femtocell placed at a fixed location inside an empty office. The validity of the FDTD method was checked by comparing numerical results of electric field distributions with measurement data obtained using a Narda Model NBM-3006 high frequency selective radiation meter [26]. After validating the accuracy of the FDTD method, the FDTD method was used to calculate electric field distributions for the LTE femtocell placed at the center of a horizontal plane with a distance of 1.0 m from the ceiling inside the office with and without the presence of 20 people and furniture. Localized SARs induced in 20 people were also calculated for the 20 people standing up and sitting on 20 metallic chairs in front of 20 wooden desks inside the office. Numerical results of localized SARs were used to verify whether the office complies with safety standards and guidelines for human exposure to RF fields at frequencies of 700, 860, 1990, and 2600 MHz.

II. THE FDTD MODEL

The FDTD method [25] is a direct solution for Maxwell's time-dependent curl equations. It is based on space-time mesh sampling of the unknown electromagnetic (EM) fields within and surrounding the object of interest. Due to its accuracy and simplicity, the FDTD method has been widely applied in antenna design, electromagnetic interference (EMI), EM wave propagation and scattering problems, design of microwave circuits, photonic device design, bioelectromagnetics, and many electromagnetic problems. In the FDTD solution procedure, the coupled Maxwell's equations in differential form are solved for various points of the scatter as well as the surrounding in a time-stepping manner until converged solutions are obtained. Following Yee's notation and using centered difference approximation on both the time and space first-order partial differentiations, six finite-difference equations for six unique field components within a unit cell are obtained. In these six finite-difference equations, electric fields are assigned to half-integer (n+1/2) time steps and magnetic fields are assigned to integer (n) time steps for the temporal discretization of fields. To ensure numerical stability, the time step δ_t is set to $\delta/(2C_o)$, where δ and C_o are the cell size and the speed of light, respectively. The center difference approximation ensures that the spatial and temporal discretizations have second-order accuracy, where errors are proportional to the square of the cell size and time increment [25]. An important problem encountered in solving the time-domain electromagnetic-field equation, by the FDTD method, is the absorbing boundary conditions. Several absorbing boundary conditions (ABC) have been proposed in the FDTD method such as second-order Mur [27], and Liao [28], and perfectly matched layer (PML) [29]. Liao's ABC and PML require a lot of memory. Second-order Mur absorbing boundary conditions are among the most frequently cited, and work in many cases. In our formulation, the second-order Mur approximation of absorbing boundary conditions [27] is used for the near-field irradiation problems. The second-order Mur absorbing boundaries are employed because they do not require much memory and have a reasonable accuracy. In this study, the external absorbing boundaries are placed at a distance of 8 δ on all sides of the scattering object as shown in Fig. 1, where δ is the cell size.

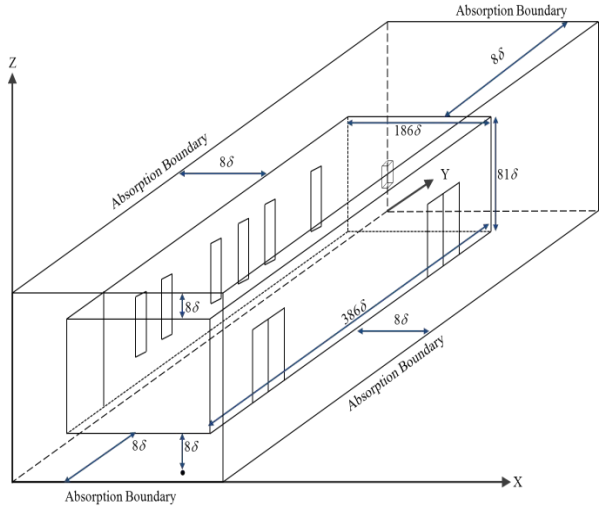

Fig. 1. FDTD model with 202×402×97=7876788 cubic cells. The cell size is 5 cm.

III. DESCRIPTION OF THE OFFICE AND LTE FEMTOCELL

Research work was conducted in an office on the tenth floor of building 7 at Yuan Ze University as shown in Fig. 2. The office has a dimension of 19×9×3.65 m and consists of two reinforced concrete slabs (ceiling and floor) with a thickness of 20 cm, two reinforced concrete walls with a thickness of 15 cm, two concrete block walls with a thickness of 15 cm, two wooden doors with a thickness of 5 cm, seven glass windows with a thickness of 1 cm, and four square reinforced concrete columns with a side length of 80 cm. The floor plan and detail dimensions of the empty office are shown in Fig. 2 (b). Relative dielectric constants and conductivities of various materials used for constructing the office at frequencies of 700, 860, 1990, and 2600 MHz [30-35] are listed in Table 1. Figure 3 (a) shows a LTE femtocell

consisting of four larger and four smaller dipole radiators designed for operating at frequencies of 698~960 and 1710~2700 MHz, respectively. The larger and the smaller radiators have dimensions of 11×3 and 4×1.5 cm respectively. The larger and smaller radiators are mounted on two different metallic plates with heights of 10 and 5 cm, respectively. Metallic plates are designed to increase the electric field strength in air. The larger and smaller metallic plates have dimensions of 30×30 and 15×15 cm, respectively. Two large radiators are opposite each other and are separated by a distance of 18 cm, and two small radiators, also opposite each other, have a distance of 8.2 cm between them. The LTE femtocell is designed to have radiation patterns normal to metallic plates with a gain of 6.1~9.8 dBi in frequency bands of 698~960 and 1710~2700 MHz.

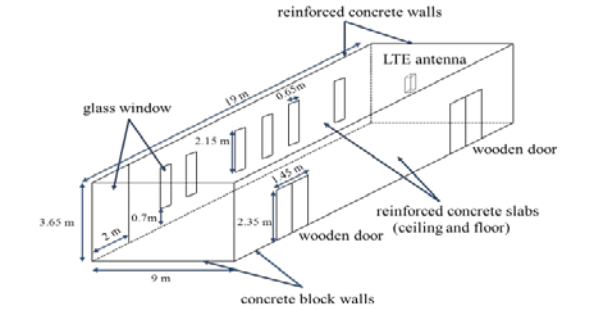

(a) Illustration of the office

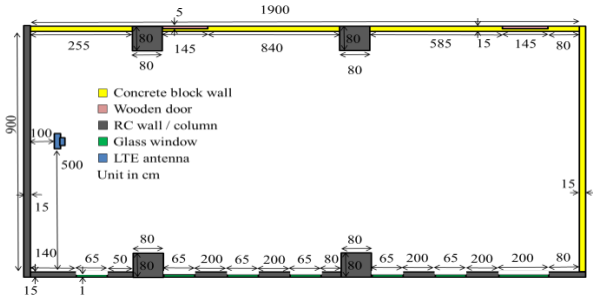

(b) Floor plan of the office with indication of the LTE femtocell

Fig. 2. The office and dimensions of walls, windows, doors, columns, and slabs.

IV. SIMULATION AND MEASUREMENT

Measurements of electric fields emitted from the LTE femtocell, placed at a height of 1.0 m above the floor on the left-hand side of the empty office as shown in Fig. 2 (b), were made at 700, 860, 1990, and 2600 MHz. The LTE femtocell was fed with a continuous sine wave generated from a signal generator Anritsu MG3694B at frequencies of 700, 860, 1990, and 2600 MHz. The emitting power of the LTE femtocell was set to be 10 dBm. Electric fields on a horizontal plane with a height of 1 m above the floor inside the empty office were measured by using a Narda Model NBM-3006 high frequency selective radiation meter. The Narda Model NRM-3006, having an isotropic E-field probe with three axis antennas, is designed to measure RF and microwave fields over the frequency range from 27 MHz to 6.0 GHz. The Narda Model NBM-3006 has an ultra-wide dynamic range from 50 V/m to 200 V/m for the frequency range of 27 MHz-6.0 GHz. Before starting measurements, a fast frequency scanning had been performed to ensure that background signals were excluded and measured frequencies were clean. In measurement, any two adjacent test points were kept at a distance of 50 cm and the Narda Model NRM-3006 was set by a very narrow-band of 1 kHz for each measured frequency. Maximum-hold measurements of all present signals were executed for about 3 minutes at each measured location. It took about 32 hours to measure electric fields at 684 grid points in the empty office for each frequency.

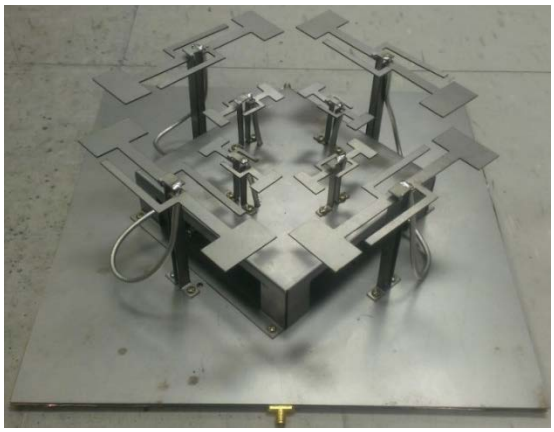

(a) The LTE femtocell

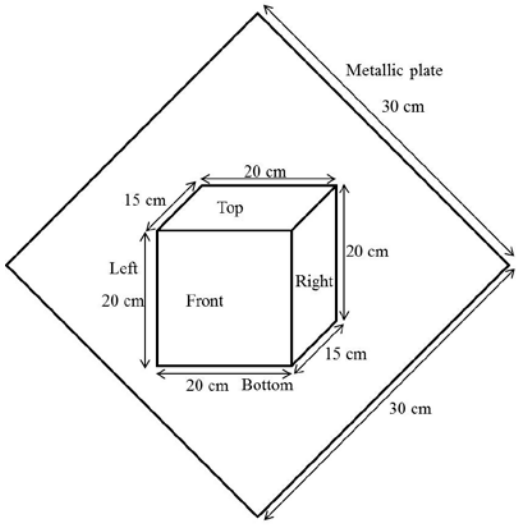

(b) Measurement locations of source fields at front, left, right, top, and bottom surfaces

Fig. 3. Picture of the LTE femtocell and locations of source fields.

In order to model the entire problem space with a uniform cell size of 5 cm, the spaces occupied by the LTE femtocell and the glass window were replaced by two different equivalent materials with many uniform cells. The equivalent material is obtained by the effective material property technique [36]. The formula of the effective material property technique is described as following:

$$\varepsilon_{eq}^{*} = \varepsilon_{air} + \frac{3V_f \times \varepsilon_{air}(\varepsilon_{m/g}^{*} - \varepsilon_{air})/(\varepsilon_{m/g}^{*} + 2\varepsilon_{air})}{1 - V_f(\varepsilon_{m/g}^{*} - \varepsilon_{air})/(\varepsilon_{m/g}^{*} + 2\varepsilon_{air})} = \varepsilon_{eq}^{'} - j\varepsilon_{eq}^{''}, \quad (1)$$

where ε_{air} and V_f are the relative dielectric constant of air and volume fraction occupied by the metallic material or the glass in a unit volume, $\varepsilon_{eq}^{'}$ and $\varepsilon_{eq}^{''}$ are the real and imaginary parts of the equivalent complex relative permittivity ε_{eq}^{*}, and $\varepsilon_{m/g}^{*}$ is the complex relative permittivity of the metallic material or the glass, respectively. It should be noted that, the imaginary part of ε_{eq}^{*} can be expressed by $\varepsilon_{eq}^{''} = \frac{\sigma_{eq}}{\omega\varepsilon_0}$, where σ_{eq} is the conductivity of an equivalent material, ω is the angular frequency, ε_0 is the dielectric constant of air, respectively. Equivalent materials in the spaces occupied by the LTE femtocell and the glass window were obtained by assuming volume fractions of 0.023 and 0.20 for the copper and the glass, respectively. Relative dielectric constants and conductivities of the equivalent materials in the spaces occupied by the LTE femtocell and the glass window are listed in Table 1. The office model has 202×402×97=7876788 cubic cells with cell size of 5 cm. For FDTD simulations, the measurement results of electric fields in the vicinity of the LTE femtocell were used as the initial sinusoidal time varying electric fields (source fields) in the FDTD model. The measurement locations of source fields at front, left, right, top, and bottom surfaces are shown in Fig. 3 (b). The measured electric fields in the vicinity of the LTE femtocell in x-, y-, and z-axis at various frequencies are listed in Table 2. In FDTD simulations, all materials were assumed to be non-magnetic (μ_r = 1.0). Simulation and measurement results of electric field distributions on a horizontal plane with a height of 1 m above the floor inside the empty office at 700, 860, 1990, and 2600 MHz are shown in Figs. 4-7. It took about 2-4 hours to run a FDTD simulation with 7876788 cubic cells in a HP work station depending on the frequency to be simulated. From Figs. 4-7, it is shown that measurement data make a good agreement with simulation results. It is also found that the field strength near the LTE femtocell has a maximum value of about 15 dBV/m and decays rapidly to about -30 dBV/m as the separation distance from the LTE femtocell increases from 0 to 19 m.

Table 1: Relative dielectric constants and conductivities of various materials

Frequency	700 MHz		860 MHz		1990 MHz		2600 MHz	
Materials	ε_r	$\sigma(S/m)$	ε_r	$\sigma(S/m)$	ε_r	$\sigma(S/m)$	ε_r	$\sigma(S/m)$
Glass	5.22	5.71×10^{-4}	5.21	7.04×10^{-4}	5.19	1.90×10^{-3}	5.17	2.93×10^{-3}
Space occupied by glass	1.40	2.53×10^{-5}	1.40	3.12×10^{-5}	1.39	8.48×10^{-5}	1.39	1.31×10^{-4}
Wood	2.99	8.51×10^{-3}	2.98	1.10×10^{-2}	2.96	2.26×10^{-2}	2.95	3.14×10^{-2}
Concrete block	4.75	9.73×10^{-3}	4.62	1.31×10^{-2}	4.53	2.70×10^{-2}	4.42	4.02×10^{-2}
RC wall/ Slab/Column	6.25	1.16×10^{-2}	6.13	3.25×10^{-2}	5.98	6.51×10^{-2}	5.90	1.02×10^{-1}
Iron	1.00	1.07×10^{7}	1.00	1.07×10^{7}	1.00	1.07×10^{7}	1.00	1.07×10^{7}
Copper	1.00	5.80×10^{7}	1.00	5.80×10^{7}	1.00	5.80×10^{7}	1.00	5.80×10^{7}
Space occupied by femtocell	1.07	5.67×10^{-12}	1.07	8.56×10^{-12}	1.07	4.58×10^{-11}	1.07	7.82×10^{-11}
Muscle	55.8	0.88	55.2	0.93	53.3	1.59	52.49	1.83
Computer case	1.00	1.07×10^{7}	1.00	1.07×10^{7}	1.00	1.07×10^{7}	1.00	1.07×10^{7}
Epoxy resin substrate	4.15	3.12×10^{-3}	4.13	3.71×10^{-3}	4.04	8.06×10^{-3}	3.99	1.02×10^{-2}
Plastics	2.54	3.32×10^{-5}	2.51	3.96×10^{-5}	2.35	8.58×10^{-5}	2.25	1.09×10^{-4}
Equivalent material of computer case	1.06	2.66×10^{-11}	1.06	4.01×10^{-11}	1.06	2.15×10^{-10}	1.06	3.66×10^{-10}
Interior of computer	1.47	1.53×10^{-4}	1.46	1.83×10^{-4}	1.46	4.10×10^{-4}	1.45	5.28×10^{-4}
Monitor	1.72	8.16×10^{-6}	1.71	9.85×10^{-6}	1.66	2.26×10^{-5}	1.63	2.99×10^{-5}

After checking the accuracy of the FDTD method, the FDTD method was used to study electric field distributions on a horizontal plane with a height of 1.0 m above the floor of the office with and without the presence of 20 people and furniture. In the study, a homogeneous model having a height of 180 cm and constructed with 808 cubical cells was used to model a standing or sitting person as shown in Fig. 8. To ensure an exposure minimization and to provide a more homogeneous field strength distribution (better signal coverage) in the office, the LTE femtocell was placed near the center of a horizontal plane having a distance of 1.0 m from the ceiling. The 20 people were simultaneously assumed to stand up or sit on 20 metallic chairs in front of 20 wooden desks as shown in Fig. 9. Figure 10 shows a computer model consisting of a mainframe and one monitor used for FDTD simulations. Equivalent electric properties of the interior of the mainframe are obtained from the effective material property technique [36] by assuming volume fractions of 0.1, 0.4, and 0.5 for the copper, epoxy resin substrates, and air located inside the interior of the mainframe, respectively. Equivalent electric properties of the computer case are obtained by assuming volume fractions of 0.02 and 0.98 for the iron and air, respectively. Equivalent electric properties of the monitor are obtained by assuming volume fractions of 0.05, 0.35, and 0.6 for the copper, plastics, and air occupied in the monitor, respectively. Relative dielectric constants and conductivities of various equivalent materials used for constructing the computer at frequencies of 700, 860, 1990, and 2600 MHz [30-35] are listed in Table 1. Figures 11-14 show the comparison of electric field distributions on a horizontal plane with a height of 1.0 m above the floor for the office with and without the presence of 20 people and furniture at 700, 860, 1990, and 2600 MHz, respectively. It is clear that the presence of 20 people and furniture affects distribution of the electric field strengths inside the office. The electric field strengths in the vicinity of 20 wooden desks have 5-10 dBV/m drops due to the impact of shadowing effect of the 20 people and furniture as shown in Figs. 11-14. It is also found that the electric field strength in the back of a metallic chair has a very low value of about -100 dBV/m. From Figs. 11-14, electric field strengths at most locations on the horizontal plane with a height of 1.0 m above the floor for the office with and without the presence of 20 people and furniture are found in the range of -10 to -30 dBV/m at 700, 860, 1990, and 2600 MHz. Since the basic sensitivity requirement for a user terminal is -83.61 dBV/m (based on -110 dBm which is corresponding to a power density of 5.8×10^{-12} W/m^2 [33]), the minimum electric field strength of -30 dBV/m obtained inside the office means a good signal will be picked up in the office. According to ANSI/IEEE standards for public exposure in uncontrolled environments, the maximum permissible exposure at frequencies of 700-2600 MHz should be below 4.6-17.3 W/m^2. It is clear that the maximum power density emitted from the LTE femtocell is about 1.326×10^{-4} W/m^2 (converted from -10 dBV/m) which is far below the ANSI/IEEE standard for public exposure.

Table 2: Measured electric fields in the vicinity of the femtocell in x-, y-, z-axis at frequencies of 700, 860, 1990, and 2600 MHz. Locations of E-field sources related to the x, y, and z coordinates are front surface (92~95, 360, 24~28) δ, left surface (92, 361~362, 24~28) δ, right surface (95, 361~362, 24~28) δ, top surface (92~95, 360~362, 29) δ, and bottom surface (92~95, 360~362, 23) δ. The cell size δ is 5 cm

	700 MHz					860 MHz				
E-field (V/m)	Front	Left	Right	Top	Bottom	Front	Left	Right	Top	Bottom
E_x	4.17	1.23	1.77	1.80	2.67	5.92	0.48	2.72	1.27	1.95
E_y	1.82	1.41	1.69	0.67	1.31	3.88	1.22	2.12	1.67	1.39
E_z	1.70	0.43	0.84	2.09	1.19	4.65	0.20	0.97	0.75	2.13
	1990 MHz					2600 MHz				
E-field (V/m)	Front	Left	Right	Top	Bottom	Front	Left	Right	Top	Bottom
E_x	5.01	0.41	0.94	0.43	1.00	6.17	0.69	1.66	0.50	1.31
E_y	2.43	0.10	0.55	0.39	0.49	5.63	0.41	0.76	1.09	0.50
E_z	4.40	0.12	0.13	0.73	1.09	4.35	0.61	0.56	0.58	1.68

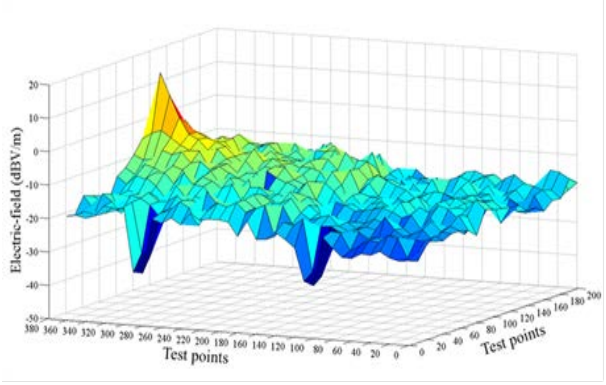

(a) Measurement

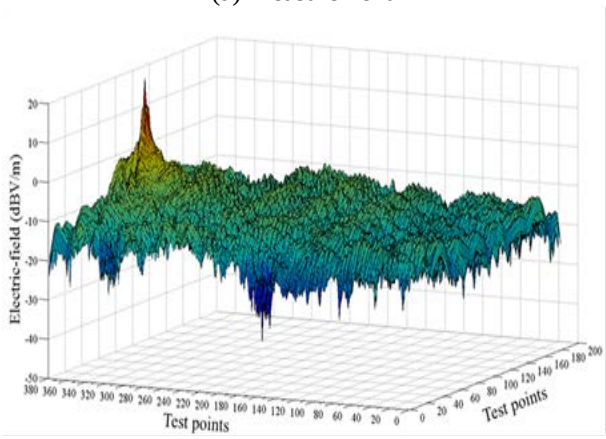

(b) Simulation

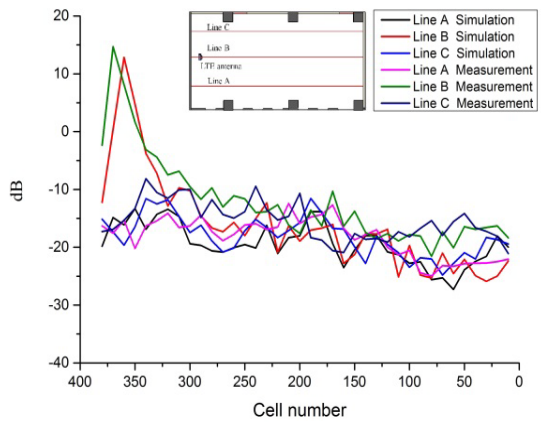

(c) Comparison of measured and simulated electric fields at lines A, B, and C

Fig. 4. Measurement and simulation results of electric field distributions on a horizontal plane with a height of 1 m above the floor inside the empty office at 700 MHz.

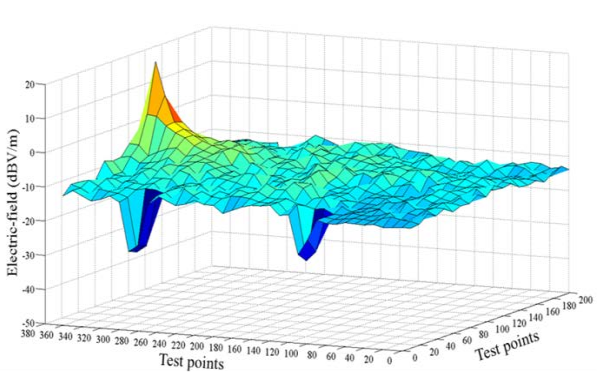

(a) Measurement

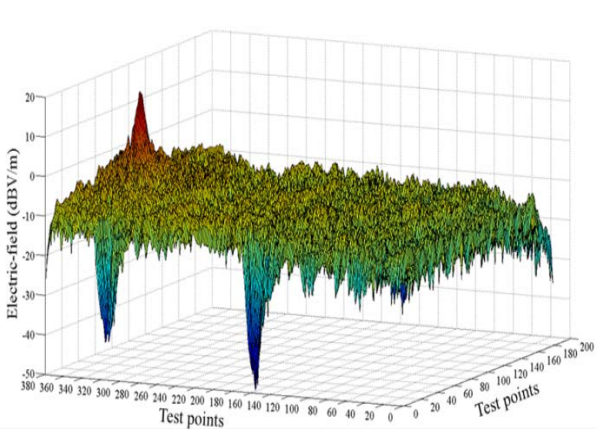

(b) Simulation

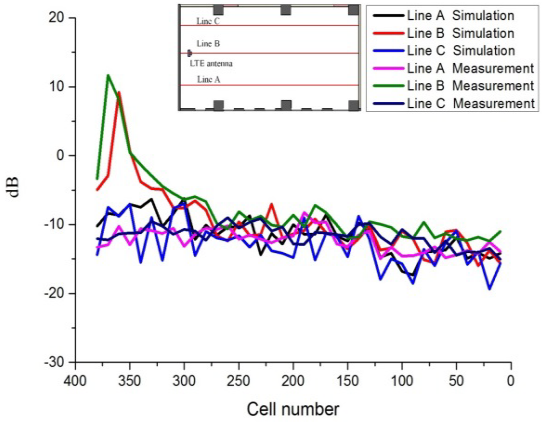

(c) Comparison of measured and simulated electric fields at lines A, B, and C

Fig. 5. Measurement and simulation results of electric field distributions on a horizontal plane with a height of 1 m above the floor inside the empty office at 860 MHz.

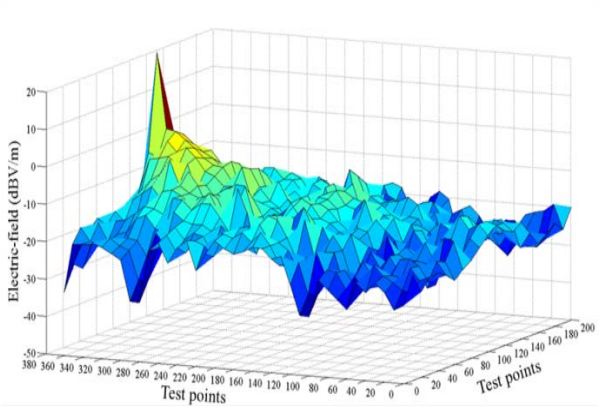

(a) Measurement

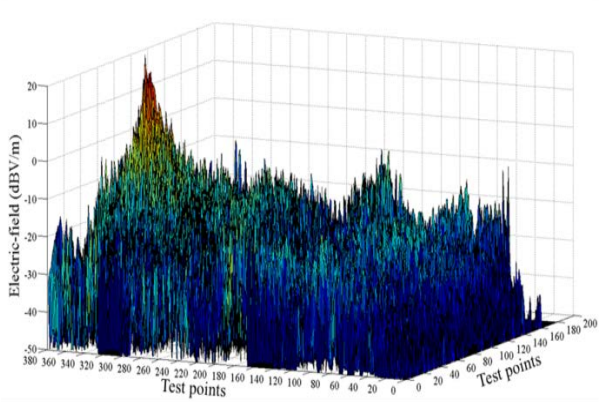

(b) Simulation

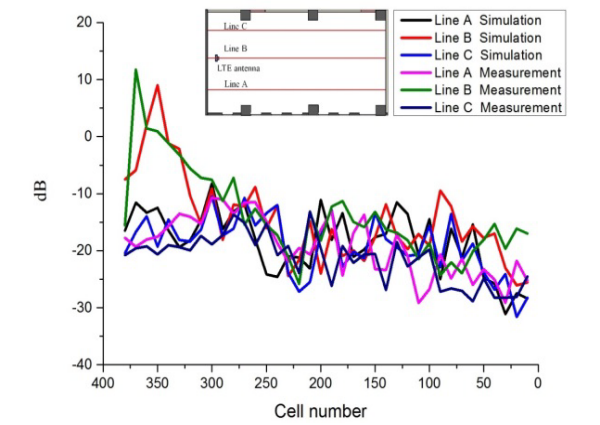

(c) Comparison of measured and simulated electric fields at lines A, B, and C

Fig. 6. Measurement and simulation results of electric field distributions on a horizontal plane with a height of 1 m above the floor inside the empty office at 1900 MHz.

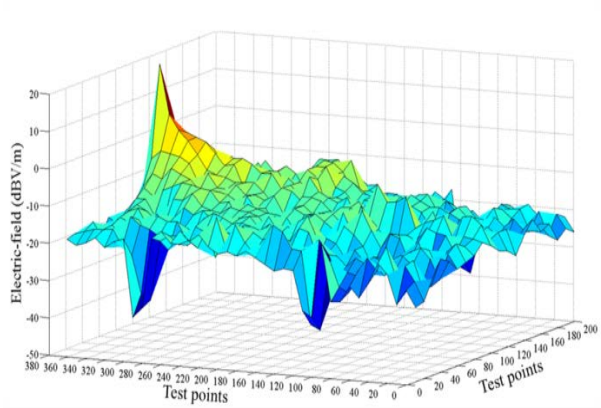

(a) Measurement

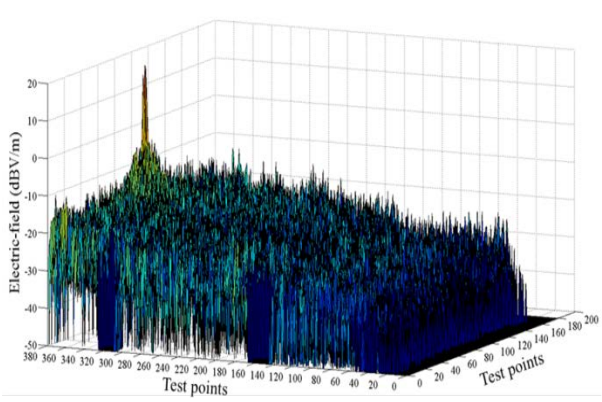

(b) Simulation

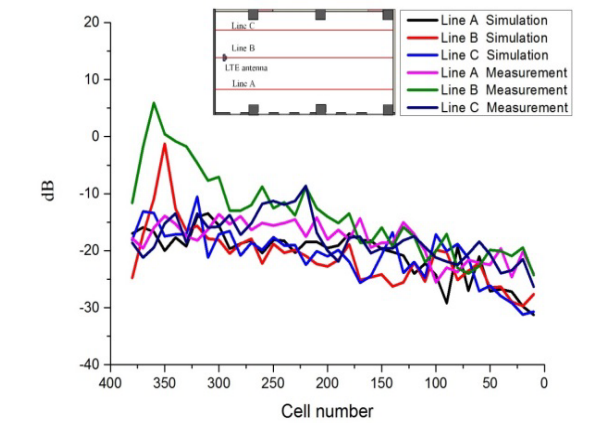

(c) Comparison of measured and simulated electric fields at lines A, B, and C

Fig. 7. Measurement and simulation results of electric field distributions on a horizontal plane with a height of 1 m above the floor inside the empty office at 2600 MHz.

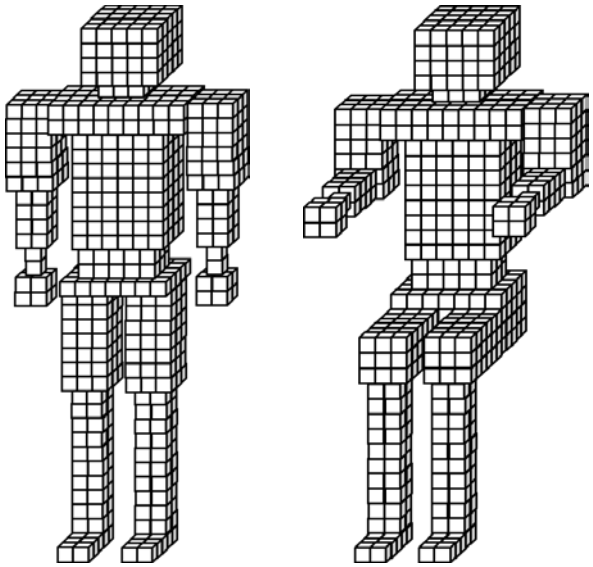

(a) Standing up (b) Sitting on a chair

Fig. 8. A homogeneous human model constructed with 808 cubical cells. The cell size is 5 cm.

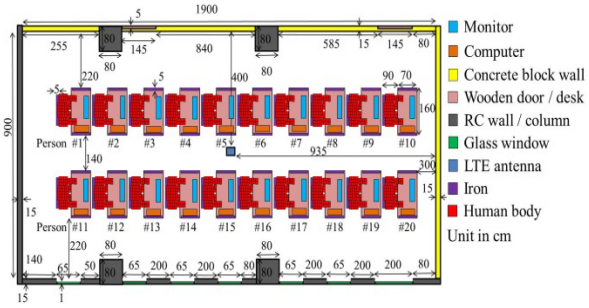

Fig. 9. Locations of 20 people and furniture inside the office.

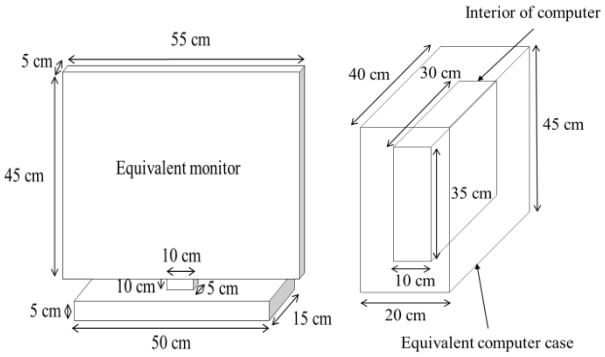

(a) Monitor (b) Mainframe

Fig. 10. A computer model used for FDTD simulations.

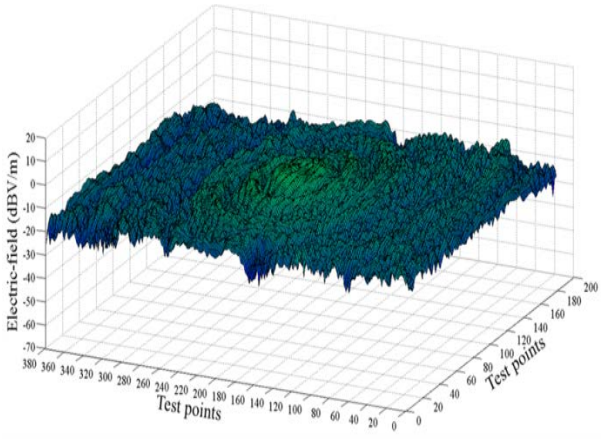

(a) Empty office

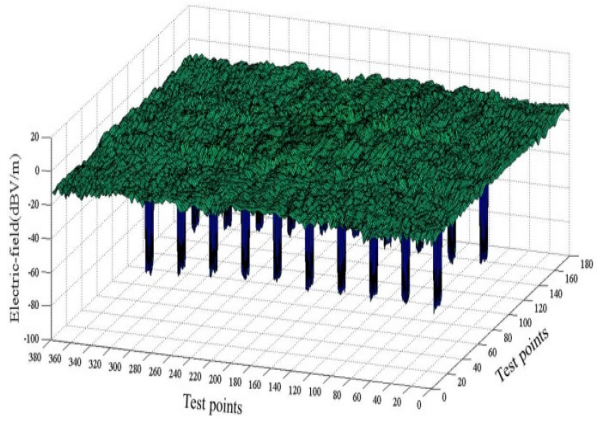

(b) 20 people sitting on metallic chairs

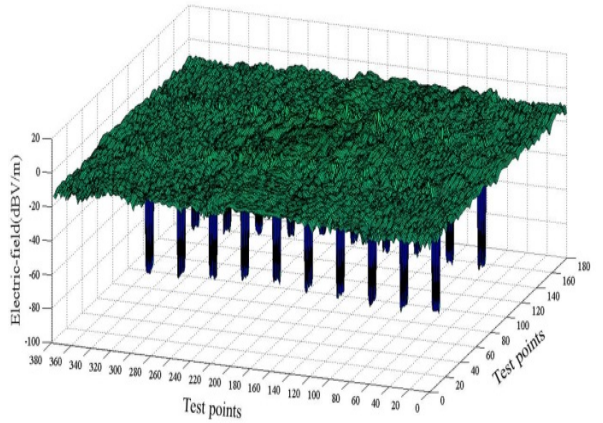

(c) 20 people standing up

Fig. 11. Comparison of electric field distributions on a horizontal plane with a height of 1.0 m above the floor for the office with and without the presence of 20 people and furniture at 700 MHz.

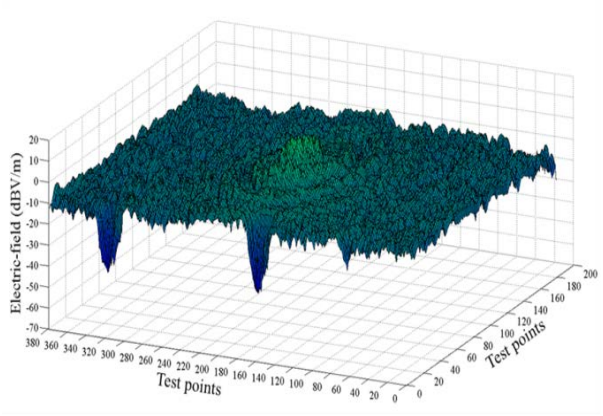

(a) Empty office

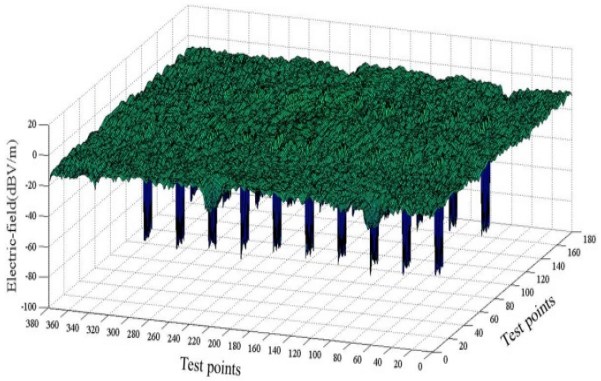

(b) 20 people sitting on metallic chairs

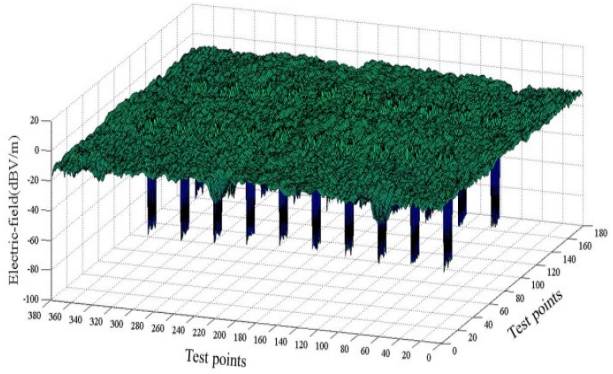

(c) 20 people standing up

Fig. 12. Comparison of electric field distributions on a horizontal plane with a height of 1.0 m above the floor for the office with and without the presence of 20 people and furniture at 860 MHz.

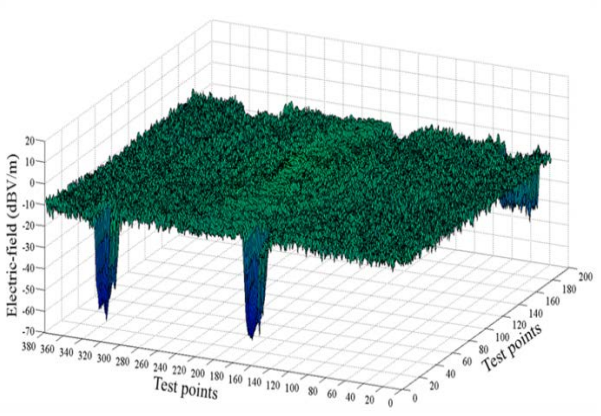

(a) Empty office

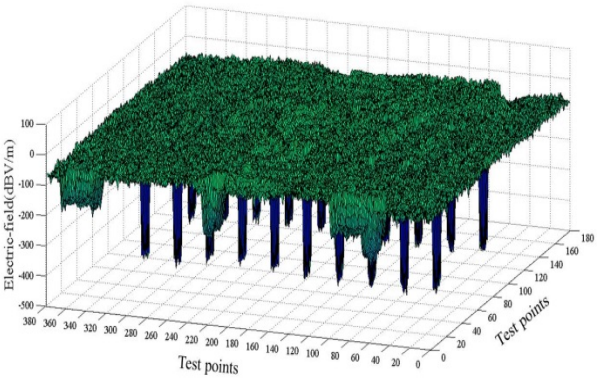

(b) 20 people sitting on metallic chairs

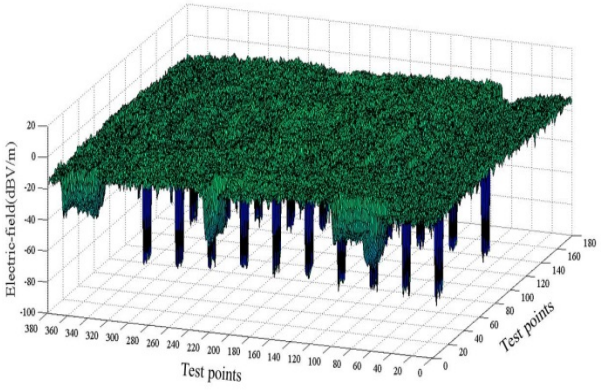

(c) 20 people standing up

Fig. 13. Comparison of electric field distributions on a horizontal plane with a height of 1.0 m above the floor for the office with and without the presence of 20 people and furniture at 1990 MHz.

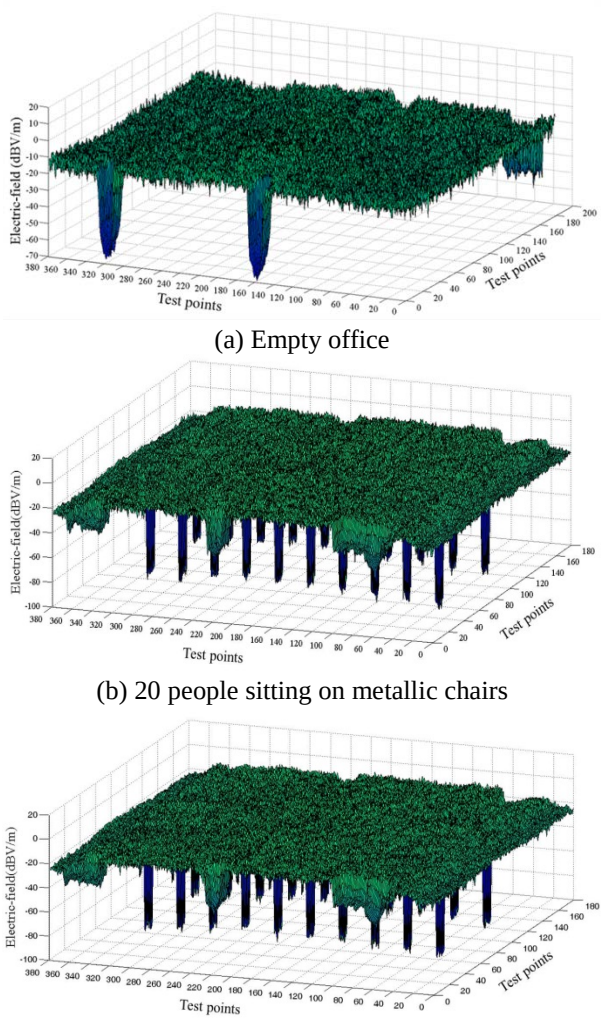

(a) Empty office

(b) 20 people sitting on metallic chairs

(c) 20 people standing up

Fig. 14. Comparison of electric field distributions on a horizontal plane with a height of 1.0 m above the floor for the office with and without the presence of 20 people and furniture at 2600 MHz.

In addition, the EM absorption in 20 people was also studied. The dielectric constants and conductivities of muscle tissue used for the homogeneous human model at various frequencies were obtained from the published literature [38] as shown in Table 1. The mass density of muscle was adopted to be 1040 kg/m^3. The human body was assumed to stand up or sit on a metallic chair in front of a wooden desk. After having obtained the induced electric field by the FDTD method, the localized SAR in each human body was calculated by the following equation:

$$\mathrm{SAR} = \sigma E^2 / 2\rho \qquad \mathrm{W/kg}, \qquad (2)$$

where σ, ρ, and E are the conductivity, mass density of muscle, and electric field induced in the human body, respectively. N = 808 is total number of cubical cells used in a human model. Figures 15-18 show localized SARs induced in the 20 people at 700, 860, 1990, and 2600 MHz, respectively. It is found that the maximum localized SARs of 1.07×10^{-5} and 9.14×10^{-6} W/kg are induced in the person numbered 5 when standing up and sitting on a metallic chair at 860 MHz, respectively. The minimum localized SARs of 4.03×10^{-11} and 2.21×10^{-11} W/kg are induced in the person numbered 12 when standing up and sitting on a metallic chair at 2660 MHz, respectively. From Figs. 15-18, it is obvious that standing people tend to have a higher SAR value than sitting people. This is because a standing person is much closer to the LTE femtocell than a sitting person. It is clear that the maximum localized SAR of 1.04×10^{-5} W/kg induced in the standing person numbered 5 is far below the ANSI/IEEE safety standard of 1.6 W/kg for public exposure in uncontrolled environments. Furthermore, the maximum localized SAR of 1.04×10^{-5} W/kg is also far below the SAR levels of 1-4 W/kg which can be subject to biological effects [39].

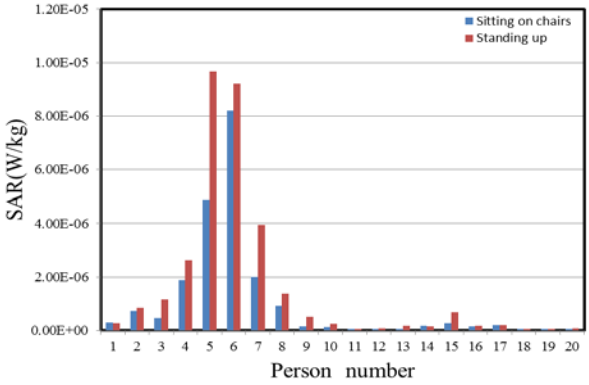

Fig. 15. Localized SARs induced in 20 people standing up and sitting on metallic chairs at 700 MHz.

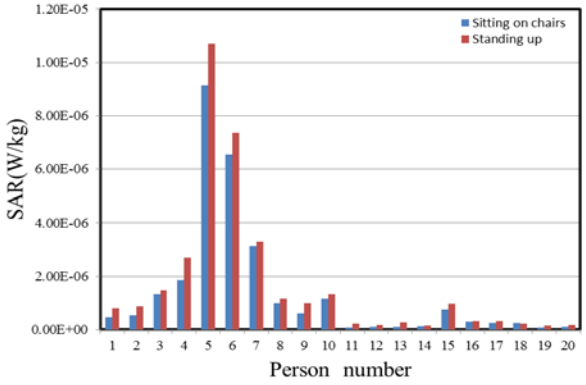

Fig. 16. Localized SARs induced in 20 people standing up and sitting on metallic chairs at 860 MHz.

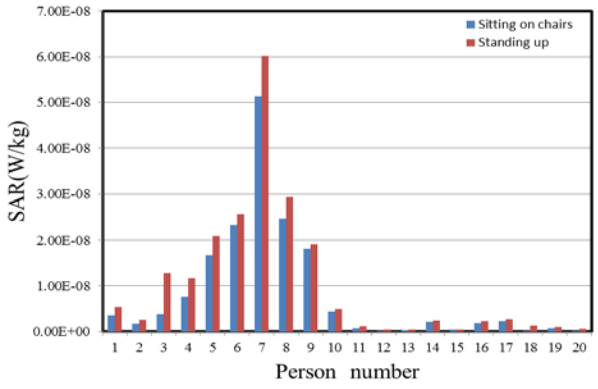

Fig. 17. Localized SARs induced in 20 people standing up and sitting on metallic chairs at 1990 MHz.

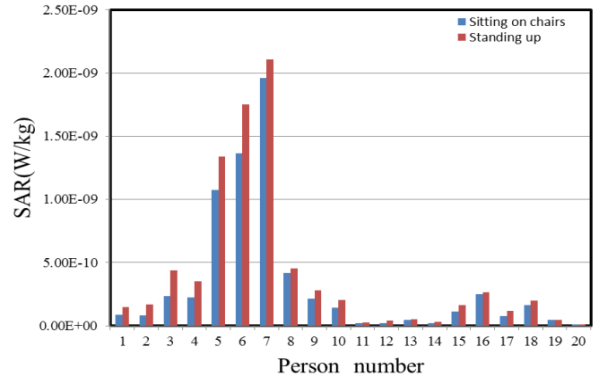

Fig. 18. Localized SARs induced in 20 people standing up and sitting on metallic chairs at 2600 MHz.

V. CONCLUSIONS

In this paper, the FDTD method was first proposed to calculate electric field distributions inside an empty office for a LTE femotcell placed at the left-hand-side of the office at frequencies of 700, 860, 1990, and 2600 MHz. The measurements of electric field distributions inside the empty office were carried out by a Narda Model NBM-3006 high frequency selective radiation meter. The validity of simulation results of electric field distributions is further checked by measurement data. After validating the accuracy of the FDTD method, the FDTD method was used to calculate electric field distributions on a horizontal plane with a height of 1 m above the floor of the office with and without the presence of 20 people and furniture for the LTE femtocell placed near the center of a horizontal plane with a distance of 1.0 m from the ceiling and transmitting a power of 10 dBm. It is found that furniture and people's existence affects distribution of the electric field strengths inside the office. The electric field strengths in the vicinity of 20 wooden desks have 5-10 dBV/m drops due to the impact of shadowing effect of 20 people and furniture. EM field distribution and variability are an important issue in the design of indoor wireless networks. Simulated electric fields at most of all locations on the horizontal plane with a height of 1.0 m above the floor for the office with and without the presence of 20 people and furniture are found in the range of -10 to -30 dBV/m which means a good signal will be picked up in the office. According to ANSI/IEEE standards for public exposure in uncontrolled environments, the maximum power density of 1.326×10^{-4} W/m^2 emitted from the LTE femtocell is far below the ANSI/IEEE safety standard of 4.6-17.3 W/m^2 for public exposure at frequencies of 700-2600 MHz. Localized SARs induced in the 20 people due to radiation from the LTE femtocell were also evaluated. It is found that the maximum localized SAR of 1.04×10^{-5} W/kg is induced in the person numbered 5 when standing up at 860 MHz. The minimum localized SAR of 7.67×10^{-12} W/kg is induced in the person numbered 12 when sitting on a metallic chair at 2660 MHz. It is found that standing people tend to have a higher SAR value than sitting people. This is because a standing person is much closer to the LTE femtocell than a sitting person. It is also found that the maximum localized SAR of 1.04×10^{-5} W/kg induced in a standing person is far below the ANSI/IEEE safety standard of 1.64 W/kg for public exposure in uncontrolled environments. Knowledge of electric field distributions and RF exposures is useful for indoor wireless network planning. The FDTD method provides a time efficient and cost effective solution for calculating electric fields emitted from LTE femtocells inside an office environment without measurements and for checking the EM absorption for public exposure to LTE femtocells.

ACKNOWLEDGMENT

The authors would like to thank Professor Heng-Tung Hsu of the Department of Communications Engineering, Yuan Ze University for providing the LTE femtocell for this study.

REFERENCES

[1] *LTE-Advanced: The 3rd Generation Partnership Projected*, 2011 [Online]. Available: http://www.3gpp.org/LTE-Advanced

[2] S. Sesia, I. Toufik, and M. Baker, *LTE-The UMTS Long Term Evolution-From Theory to Practice*, 2nd ed. including Release 10 for LTE-Advanced, New York: John Wiley & Sons, 2011.

[3] F. Khan, *LTE for 4G Mobile Broadband-Air Interface Technologies and Performance*, Cambridge University Press, New York, 2009.

[4] G. M. Whitman, K.-S. Kim, and E. Niver, "A theoretical model for radio signal attenuation inside buildings," *IEEE Trans. Veh. Technol.*, vol. 44, no. 3, pp. 621-629, 1995.

[5] R. P. Torres, L. Valle, M. Domingo, and M. C. Diez, "CINDOOR: An engineering tool for planning and design of wireless systems in enclosed spaces," *IEEE Antennas Propagat. Mag*., vol. 41, no. 4, pp. 11-22, 1999.

[6] Z. Ji, B. H. Li, H. X. Wang, H. Y. Chen, and T. K. Sarkar, "Efficient ray-tracing methods for propagation prediction for indoor wireless communications," *IEEE Antennas Propagat. Mag.*, vol. 43, no. 2, pp. 41-49, 2001.

[7] A. Aragon-Zavala, B. Belloul, V. Nikolopoulos, and S. R. Saunders, "Accuracy evaluation analysis for indoor measurement-based radio-wave-propagation predictions," *IEE Proc.-Microw. Antennas Propag.*, vol. 153, no. 1, Feb. 2006.

[8] X. Ling and K. L. Yeung, "Joint access point placement and channel assignment for 802.11 wireless LANs," *IEEE Trans. Wireless Commun.*, vol. 5, no. 10, pp. 2705-2711, Oct. 2006.

[9] D. Plets, W. Joseph, K. Vanhecke, E. Tanghe, and L. Martens, "Simple indoor path loss prediction algorithm and validation in living lab setting," *Wireless Pers. Commun.*, vol. 68, pp. 535-552, 2013.

[10] V. Degli-Esposti, G. Falciasecca, F. Fuschini, and E. M. Vitucci, "A meaningful indoor path-loss formula," *IEEE Antennas Wireless Propag. Lett*., vol. 12, pp. 872- 875, 2013.

[11] M. Ayadi and A. Ben Zineb, "Body shadowing and furniture effects for accuracy improvement of indoor wave propagation model," *IEEE Trans. Wireless Commun*., vol. 13, no. 11, pp. 5999-6006, Nov. 2014.

[12] NCRP, "Biological effects and exposure criteria for radiofrequency electromagnetic fields," NCRP Rep. 86, 1986.

[13] *IEEE Standard for Safety Levels with Respect to Human Exposure to Radio Frequency Electromagnetic Fields, 3 kHz to 300 GHz*, IEEE Standard C95.1, 2005.

[14] ICNIRP, "Guidelines for limiting exposure to time-varying electric, magnetic and electromagnetic fields," *Health Phys.*, vol. 74, no. 4, pp. 494-522, Apr. 1998.

[15] P. Frei, E. Mohler, G. Neubauer, G. Theis, A. Burgi, J. Frohlich, C. Braun-Fahrlander, J. Bolte, M. Egger, and M. Roösli, "Temporal and spatial variability of personal exposure to radiofrequency electromagnetic fields," *Environ. Res.*, vol. 109, pp. 779-785, 2009.

[16] H. Y. Chen and C. Y. Chuang, "Currents induced in human bodies during RF exposure near a cellular phone base station," *Electromagn*., vol. 29, no. 1, pp. 13-23, Jan. 2009.

[17] W. Joseph, P. Frei, M. Ro¨osli, G. Vermeeren, J. Bolte, G. Thur´oczy, P. Gajsek, T. Trcek, E. Mohler, P. Juhasz, V. Finta, and L. Martens, "Between-country comparison of whole-body SAR from personal exposure data in urban areas," *Bioelectromagn.*, vol. 33, no. 8, pp. 682-694, Dec. 2012.

[18] J. Cooper, B. Marx, J. Buhl, and V. Hombach, "Determination of safety distance limits for a human near a cellular base station antenna, adopting the IEEE standard or ICNIRP guidelines," *Bioelectromagn.*, vol. 23, no. 6, pp. 429-443, 2002.

[19] T. Alanko, M. Hietanen, and P. von Nandelstadh, "Occupational exposure to RF fields from base station antennas on rooftops," *Ann. Telecommun.*, vol. 63, pp. 125-132, 2008.

[20] D. Plets, W. Joseph, K. Vanhecke, and L. Martens, "Exposure optimization in indoor wireless networks by heuristic network planning," *Progress Electromagn. Res.*, vol. 139, pp. 445-478, 2013.

[21] G. Koutitas and T. Samaras, "Exposure minimization in indoor wireless networks," *IEEE Antennas Wireless Propag. Lett.*, vol. 9, pp. 199-202, 2010.

[22] A. Bamba, W. Joseph, J. B. Andersen, E. Tanghe, G. Vermeeren, D. Plets, J. O. Nielsen, and L. Martens, "Experimental assessment of specific absorption rate using room electromagnetics," *IEEE Trans. Electromagn. Compat*., vol. 54, no. 4, pp. 747-757, Aug. 2012.

[23] A. Boursianis, P. Vanias, and T. Samaras, "Measurements for assessing the exposure from 3G femtocells," *Radiation Protection Dosimetry*, vol. 150, no. 2, pp. 158-167, 2012.

[24] A. Bamba, W. Joseph, A. Boursianis, T. Samaras, G. Vermeeren, A. Thielens, and L. Martens, "Fast assessment of RF power absorption in indoor environments by room electromagnetics theory," *Radiation Protection Dosimetry*, first published online Nov. 14, 2015.

[25] K. S. Yee, "Numerical solution of initial boundary value problems involving Maxwell's equations in isotropic media," *IEEE Trans. Antennas Propag*., vol. AP-14, no. 5, pp. 302-307, 1966.

[26] Narda Safety Test Solutions, 435 Moreland Road, Hauppauge, NY 11788, 2015.

[27] G. Mur, "Absorbing boundary conditions for the finite-difference approximation of the time-domain electromagnetic field equation," *IEEE Trans. Electromagn. Compat.*, *EMC-23*, pp. 377-382, 1981.

[28] Z. P. Liao, H. L. Wong, B. P. Yang, and Y. F. Yuan, "A transmitting boundary for transient wave analysis," *Scientia Sinica (Series A)*, vol. 27, no. 10, pp. 1063-1076, Oct. 1984.

[29] J. P. Berenger, "A perfectly matched layer for the absorption of electromagnetic waves," *J. Comp. Phys.*, vol. 114, pp. 185-200, Oct. 1994

[30] A. von Hippel, *Dielectric Materials and Applications*, The MIT Press, Cambridge, Mass., 1954.

[31] C. F. Yang, C. J. Ko, and B. C. Wu, "A free space approach for extracting the equivalent dielectric constants of the walls in buildings," *IEEE AP-S. Int. Symp. Dig.*, Baltimore, MD, vol. 2, pp. 1036-1039, July 21-26, 1996.

[32] D. J. Cichon, T. Zwick, and J. Lahteenmaki, "Ray optical indoor modeling in multi-floored buildings: simulations and measurements," In *AP-S. Digest, Antennas and Propagation Society Int. Symp.*, Newport Beach, CA, vol. 1, pp. 522-525, July 21-26, 1995.

[33] A. C. M. Austin, M. J. Neve, and G. B. Rowe, "Modeling propagation in multifloor building using the FDTD method," *IEEE Trans. Antennas Propag.*, vol. 59, no. 11, pp. 4239-4246, Nov. 2011.

[34] M. Thiel and K. Sarabandi, "3D-wave propagation analysis of indoor wireless channels utilizing hybrid methods," *IEEE Trans. Antennas Propag.*, vol. 57, no. 5, pp. 1539-1546, Nov. 2019.

[35] D. Pena, R. Feick, H. D. Hristov, and W. Grote, "Measurement and modeling of propagation losses in brick and concrete walls for 900-MHz band," *IEEE Trans. Antennas Propag.*, vol. 51, no. 1, pp. 31-39, Jan. 2003.

[36] S. K. Patil, M. Y. Koledintseva, R. W. Schwartz, and W. Huebner, "Prediction of effective permittivity of diphasic dielectrics using an equivalent capacitance model," *J. Appl. Phys.*, vol. 104, pp. 074108-1-074108-11, 2008.

[37] LessEMF.com, *Radio Frequency & Microwave Meters*, 2014 [Online]. Available: http://www. lessemf. com/rf.html

[38] A. Christ, A. Klingenbock, T. Samaras, C. Goiceanu, and N. Kuster, "The dependence of electromagnetic far-field absorption on body tissue composition in the frequency range from 300 MHz to 6 GHz," *IEEE Trans. Microw. Theory Tech.*, vol. 54, no. 5, pp. 2188-2195, May 2006.

[39] J. A. Elder and D. F. Cahill, "Biological Effects of Radiofrequency Radiation," U.S. Environmental Protection Agency, EPA Rep. no. EPA-600/8-83-026F, Research Triangle Park, NC. 1984.

Hsing-Yi Chen was born in Taiwan, in 1954. He received the B.S. and M.S. degrees in Electrical Engineering in 1978 and 1981 from Chung Yuan Christian University and National Tsing Hua University, respectively. He received the Ph.D. degree in Electrical Engineering from University of Utah, Salt Lake City, Utah in 1989. He joined the faculty of the Department of Electrical Engineering, Yuan Ze University, Taiwan, in September 1989. He was the Chairman of Electrical Engineering from 1996 to 2002, the Chairman of Communications Engineering from 2001 to 2002, the Dean of Engineering College from 2002 to 2006, the Dean of Electrical and Communication Engineering College from 2006 to 2012, and the Dean of Research and Development Office from 2012 to 2013. Currently, he is the Dean of General Affairs Office, Yuan Ze University. His current interests include electrostatic discharge, electromagnetic scattering and absorption, waveguide design, radar systems, electromagnetic compatibility and interference, bioelectromagnetics, electromagnetic radiation hazard protection, and applications of frequency selective surface.

He is a member of Phi Tau Phi. He was also a member of the editorial board of the *Journal of Occupational Safety and Health* from 1996 to 1997. He was elected an Outstanding Alumnus of the Tainan Second High School in 1995. He has been the recipient of numerous awards including the 1990 Distinguished Research, Service, and Teaching Award presented by the Yuan Ze University, the 1999 and 2002 YZU Outstanding Research Award, and the 2005 Y. Z. Hsu Outstanding Professor Award for Science, Technology & Humanity Category. He was awarded Chair Professor by Far Eastern Y. Z. Hsu Science and Technology Memorial Foundation in 2008. His name is listed in Who's Who in the World in 1998.

Shu-Huan Wen was born in Taiwan, in 1991. He received the B.S. degree in Electronic Engineering from Oriental Institute of Technology in 2013. He is currently working toward the M.S. degree in Communications Engineering at Yuan Ze University, Taiwan. His research interests include patch antenna design, frequency selective surfaces, EM field measurement, and computational electromagnetics.